# Colloidal Nanocrystals as Heterogeneous Catalysts for Electrochemical CO₂ Conversion[†]

Jianfeng Huang and Raffaella Buonsanti*

Laboratory of Nanochemistry for Energy Research, Institute of Chemical Sciences and Engineering, Ecole Politechnique Fédérale de Lausanne, Sion, CH-1950, Switzerland

**ABSTRACT:** In the past decade, atomically engineered nanomaterials with different sizes and exposed facets have been proven to be excellent model systems to advance catalytic studies. Colloidal chemistry is one of the most powerful wet-chemistry techniques to tailor-make nanomaterials, thus making colloidal nanocrystals an ideal playground to investigate structural and compositional reaction sensitivities but also to study degradation pathways. In this Perspective, we focus on colloidally synthesized nanocrystals as heterogeneous catalysts for the electrochemical CO₂ reduction reaction. We discuss very recent studies from us and from others, which encourage the scientific community to explore the tunability offered by colloidal chemistry even further. For example, synergistic interactions of the metallic nanocrystal catalyst with domains of different chemical nature could be exploited with the aim of revealing new catalytic motifs that promote the activity, selectivity, and stability of electrocatalysts for CO₂ conversion.
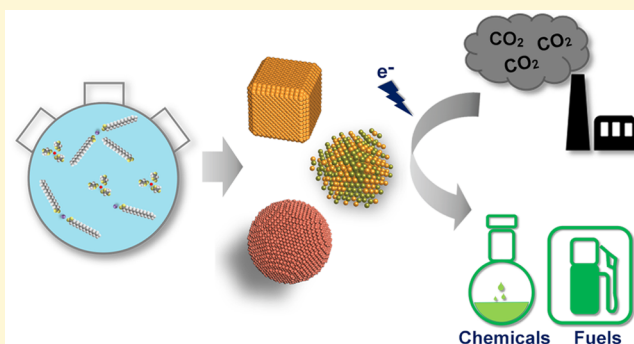
## 1. INTRODUCTION

CO₂ is an under-utilized resource for chemicals and fuels. With gigatons of this gas released in the atmosphere each year, any technology which uses CO₂ as a raw material can make a huge impact on climate change. However, the thermodynamic stability of the CO₂ molecule implies that high temperatures, highly reactive reagents (i.e., hydrogen), or a different source of energy are required to carry out its conversion. The exploitation of intermittent renewable sources (i.e., solar, wind) emerges as a win−win solution, considering the need for seasonal storage. While progress has been made, one of the main challenges is to find stable catalysts that can electrochemically reduce CO₂ with high efficiency and selectivity toward one specific product.

In this perspective, we focus on colloidally synthesized nanocrystals (NCs) as some of the most tunable and defined nanomaterials which represent a great material platform to better understand the effect of size, shape, surface chemistry, and composition on the catalytic activity, selectivity, and stability of heterogeneous catalysts for electrochemical CO₂ reduction reaction (CO₂RR). After a brief overview on the reaction mechanism and on the performance metrics, we illustrate recent contributions on the use of colloidal NCs as CO₂RR electrocatalysts from others and from us. Through a few examples, we provide a general overview of the structural and compositional tunability attainable by means of colloidal chemistry and we discuss the role played by the ligands, including the possible techniques for postsynthetic removal.

[†]This Perspective is part of the *Up-and-Coming* series.

Finally, we highlight the importance of monitoring catalyst reconstruction during operation and how the monodispersity of the colloidal nanocrystals can aid in identifying degradation pathways.

## 2. OVERVIEW OF ELECTROCHEMICAL CO₂RR

In this section, our intention is not to provide a complete review of the field but rather to highlight the challenges and the state-of-the-art and to provide the reader with the most important performance metrics useful to compare different catalysts. If the main purpose of CO₂RR is to store energy into chemical bonds, then high-energy dense molecules such as long-chain hydrocarbons become desirable.[1] Alternatively, one might tackle products which are essential basic chemicals for industry and are currently extracted from petroleum, such as ethylene and acetylene. Finally, CO might be also attractive to feed into the conventional Fischer−Tropsch process. Currently, Cu is about the only monometallic catalyst with propensity to form hydrocarbons with decent efficiencies, yet it generates 16 different products (Figure 1A).[2−4] The reaction mechanisms associated with these products are quite complex and are under investigation both theoretically and experimentally.[5−13] Figure 1B gives a simplified overview of the key reaction steps to CO, methane, and ethylene. After the first electron transfer to form the CO₂ radical anion, CO₂•⁻, the
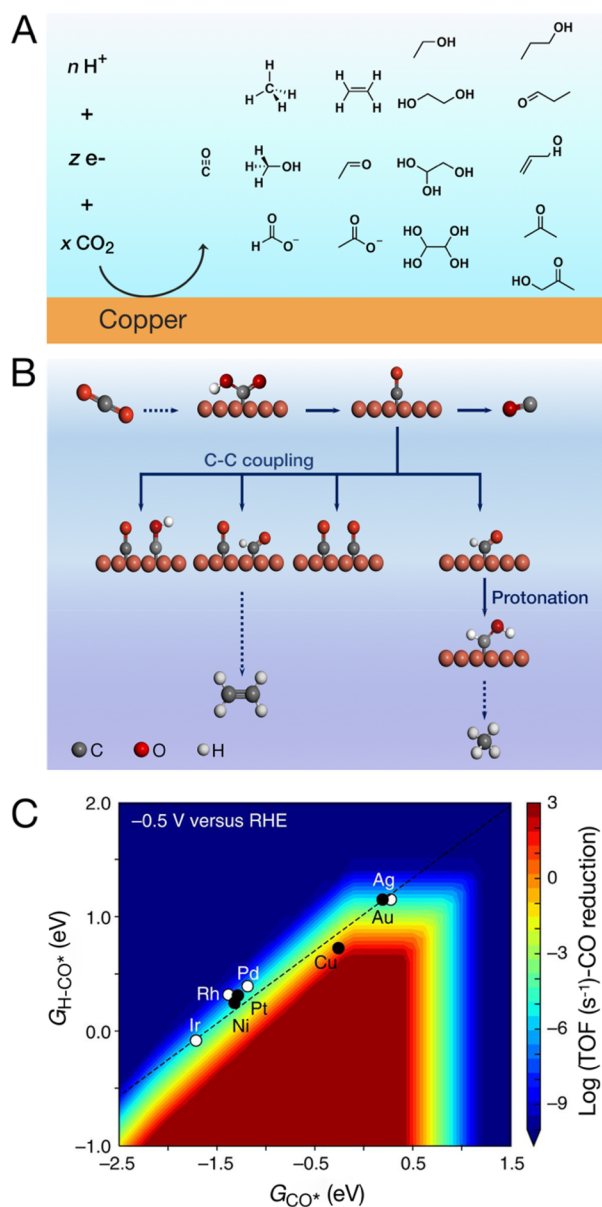
**Figure 1.** Mechanistic overview on the electrochemical $CO_2RR$. (A) Reduction products obtained from polycrystalline copper. (B) Simplified reaction pathway from $CO_2$ to CO, methane, and ethylene. The dotted arrows indicate more than one step needed to complete the pathway. (C) 2D map of the rate of CO reduction as a function of H−CO* transition state energy and CO* binding energy, with the red color corresponding to the higher reduction rate. The figure in (A) is adapted with permission from ref 2. Copyright 2012 Royal Society of Chemistry. The figure in (C) is adapted with permission from ref 6, licensed under a Creative Commons Attribution 4.0 International License http://creativecommons.org/licenses/by/4.0/. Copyright 2017 Nature Publishing Group.

formation of CO is promoted through the stabilization of the COOH* intermediate (* indicates that the molecule is adsorbed on the surface), and if CO* binds weakly to the catalyst surface, then CO evolution is observed.[5−13] If CO binds strongly enough to the surface for the reaction to move forward, then a coupled electron/proton step leads to the formation of CHO* through a (H−CO)* transition state.[6] C−C coupling and further CHO* protonation become the key steps toward ethylene and methane, respectively. The C−C

coupling mechanism is still under debate, and various $C_2$ intermediates are currently being proposed. The team led by Norskov explains the unique reactivity of copper by proposing scaling relationships between key $CO_2RR$ intermediates, deriving from the fact that they all bind to the metallic surfaces through carbon atoms.[6] Figure 1C shows the linear dependence between the (H−CO)* transition state energy and the CO binding energy: if one aims at increasing the reaction rate by stabilizing (H−CO)*, CO is also stabilized and thus poisons the catalyst surface. Among the metals, Au and Ag generate mostly CO because of the weaker binding energy (CO does not reside sufficiently long on the surface to further react). Cu is special because it exhibits the optimal binding energies for the reduction reaction to proceed past CO. Finally, one has to consider that the hydrogen evolution reaction (HER) will be always competing with $CO_2RR$. Manipulating the kinetics of the first electron step to $CO_2$ will increase the competitiveness of $CO_2RR$ over HER.[12,13]

To summarize, the community has two main challenges to solve: (1) promoting $CO_2RR$ over HER and (2) selectively targeting one $CO_2RR$ product to minimize separation costs. The strategies toward solving these challenges are multiple and include catalyst design, reactor engineering, and electrolyte modification. Eventually, all these aspects have to converge toward an industrially scalable $CO_2$ electrolyzer. One sketch of the electrochemical cell used in our group is reported in Figure 2A, and it takes inspiration from previous work by Lobaccaro et al.[14] Here, the NC catalysts deposited on glassy carbon serve as the working electrode (WE), Selemion is used as the membrane, Ag/AgCl as the reference electrode (RE), and Pt foil or C as the counter electrode (CE). In this H-type cell, the electrolyte is an aqueous potassium bicarbonate buffer solution (0.1 M $KHCO_3$, pH = 6.8), which is quite common across the literature. Nevertheless, studies have been reported which evidence the influence of the buffer (i.e., nature and capacity) and of the cations and anions (e.g., alkali ions and halide ions) on the reaction pathways.[3,15−26] Attention has been given also to the role of the pH, with lower pH favoring HER and higher pH being impeded by the bicarbonate/carbonate equilibrium.[15,16,27,28] Changes of the pH close to the catalytic surface, referred to as "local pH", have been recognized to be important in determining the reaction pathway.[29−32] Local pH will be affected by the current density that is measured, and thus higher catalyst loadings or nanostructured catalysts with different sizes and shapes might experience different surface pHs during the reaction at a fixed potential.[29] Tools to actually monitor the local pH during the reaction will certainly strengthen all the conclusions made so far. Organic solvents (e.g., dimethylformamide, acetonitrile) represent an alternative choice to aqueous solutions, as they facilitate the dissolution of $CO_2$ and allow the use of additives, i.e., ionic liquids, which have been proposed to activate $CO_2$.[33−36] Because of mass transport limitation in liquid electrolytes, the community is transitioning toward hybrid gas/liquid cells equipped with GDEs (gas diffusion electrodes) and towards fully gas-fed MEA-type (MEA= membrane electrode assembly) electrochemical reactors.[37,38] In GDEs, carbon paper and cloth substitute glassy carbon as catalyst substrates. Examples of one hybrid gas/liquid cell and one exclusively gas-fed cell from our group are shown in Figure 2B,C, respectively. The use of GDEs frees from the constrains imposed by the carbonate/bicarbonate equilibrium in water because the $CO_2$ reaches the catalyst surface as a gas. Therefore, recent studies employing
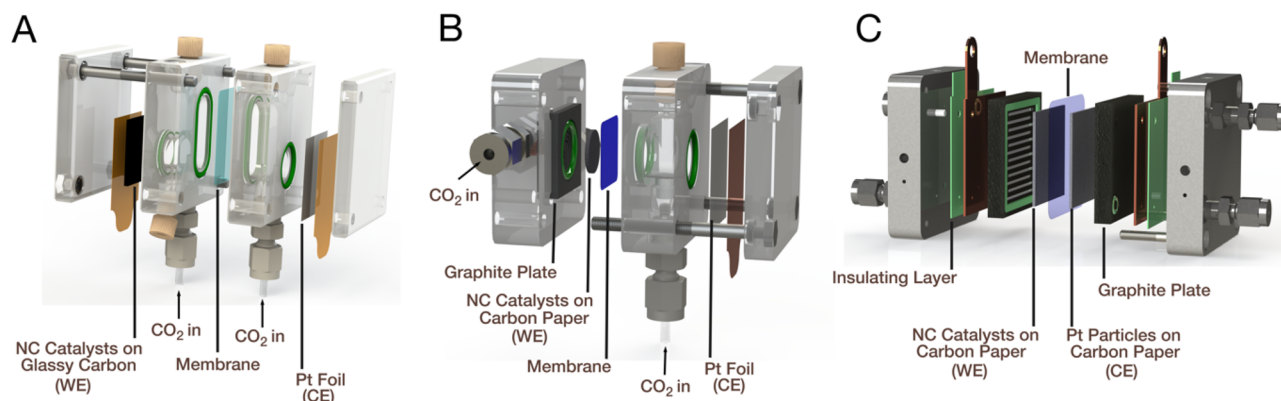
**Figure 2.** Electrochemical $CO_2RR$ cells currently used in our laboratory. (A) Liquid cell. (B) Hybrid gas/liquid cell. (C) Gas-fed cell. The graphite plates serve as gas diffusion layers. Reprinted with permission from Jérémie Bérard, Laboratory of Nanochemistry for Energy Research, EPFL.
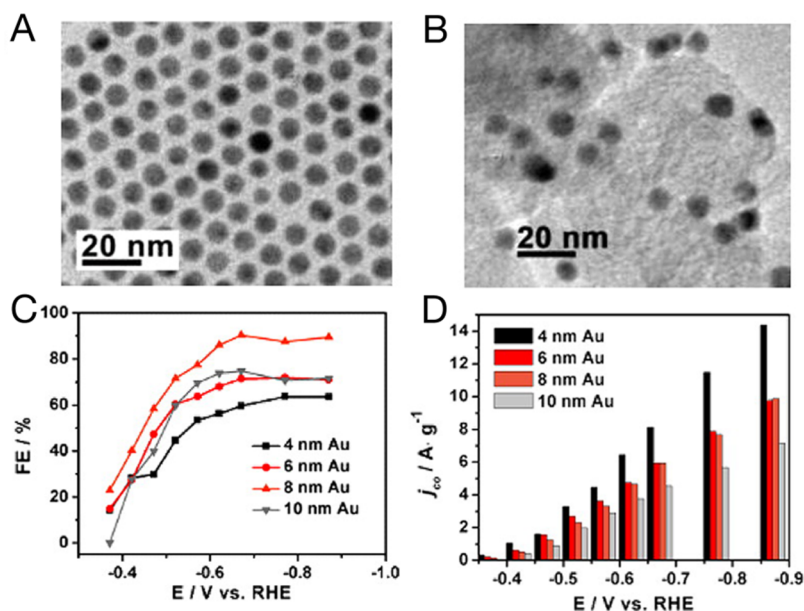


**Figure 3.** Size-dependent electrocatalytic behavior of spherical Au NCs. (A, B) TEM images of (A) the 8 nm Au NCs and (B) the C−Au NCs. (C) Potential-dependent FEs of the C−Au on electrocatalytic reduction of $CO_2$ to CO. (D) Current densities for CO formation (mass activities) on the C−Au at various potentials. Adapted with permission from ref 47. Copyright 2013 American Chemical Society.

the hybrid cell have utilized very basic solutions (up to 10 M KOH) and propose an active role of the $OH^-$ in achieving high selectivity toward ethylene and very high current densities.[38] In this perspective, we mainly focus on the discussion of $eCO_2RR$ performed in the liquid cell and in the hybrid cell in the presence of aqueous electrolytes, as these operation conditions still remain the most common so far.

When comparing the performance of $CO_2RR$ catalysts, the metric for selectivity is the Faradaic efficiency (FE), which is the fraction of Faradaic charge utilized to produce a given product. The activity corresponds to the rate of conversion, which for electrocatalysts means the converted charges over time. Thus, the overall activity of the catalyst is evaluated based on total current density at a certain potential; instead, the activity toward a particular product is extracted from the partial current density where only the charges converted in that product are counted. One important consideration is that the current density has to be normalized by the electrochemically active surface area (ECSA) to extract meaningful information. The optimal method to determine the ECSA does not exist yet; however, the commonly accepted one is from measure-

ments of the double-layer capacitance of the electrode−electrolyte interface.[39] FE and current densities are normally collected at various applied potentials, which are reported versus the reversible hydrogen electrode (RHE). The difference between the thermodynamic potential at which one product is expected to form and the actual potential at which it is detected is related to the so-called "overpotential". The lower the overpotential is, the more active the catalyst is. Due to the many products generated at the same potential in $CO_2RR$, it is difficult to extract the exact value of overpotential unless real time product detection methods, such as online electrochemical mass spectrometry, are utilized.[5]

In the following sections, we will also include a few technical details, such as electrode preparation and electrolyte composition, to highlight some of the variations in measurement conditions across the literature. These variations, together with differences in data reporting, make often challenging the comparison among different studies. Recently, the team led by Jaramillo and Bell has reported good practice for electrochemical $CO_2RR$ with the purpose of providing a

baseline for catalyst benchmarking, and we refer to this publication for details.[40]

## 3. COLLOIDAL NANOCRYSTALS AS ELECTROCATALYSTS FOR CO₂RR

**3.1. Structure/Property Relations.** Colloidal NCs have been largely explored as electrocatalysts for the oxygen reduction reaction with beautiful studies conducted by the groups led by Yang, Stamenkovic, and Strasser, among others, and as hydrogen evolution catalysts with important work done by the group led by Schaak.[41−46] Being the study of electrochemical CO₂RR a more recent field, fewer examples have been published to date. As mentioned in the previous session, Au and Ag are selective for CO, while Cu is the only metal with propensity to form hydrocarbons. Consequently, most of the studies have been conducted on Au- and Cu-based NCs with controlled sizes, shapes, and structures.

*Gold NCs.* The group led by Sun has investigated the behavior of different sized spherical Au NCs and of Au nanowires (NWs) as electrocatalysts for CO₂ reduction to CO (Figures 3 and 4).[47,48] Spherical Au NCs of 4, 6, 8, and 10 nm
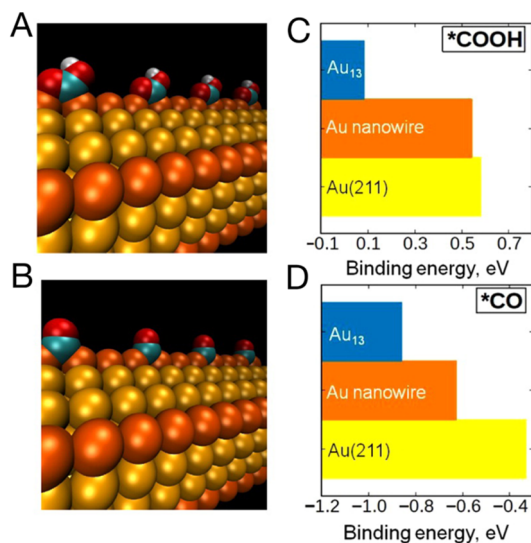


**Figure 4.** Facet-dependent electrochemical behavior in Au NWs. (A, B) Configurations of the adsorbed (A) COOH and (B) CO on Au NWs. The edge-type sites are highlighted in orange. In the Au−COOH bonding mode, both C and O (carbonyl) bind to Au directly with OH tilting away from the O=C bond. In the Au−CO bonding mode, one CO binds to two Au atoms with CO serving as the bridge. (C, D) Binding energies of the key (C) COOH and (D) CO intermediates calculated on the Au NW, Au₁₃ cluster, and Au(211). Adapted with permission from ref 48. Copyright 2014 American Chemical Society.

were tested. The electrodes were prepared by depositing the NCs on carbon black (Vulcan) and annealing at 165 °C for 12 h in order to remove the ligands, followed by the preparation of a paste made with the C−Au, PVDF (polyvinylidene fluoride), and NMP (N-methyl-2-pyrrolidone) before depositing the slurry on carbon paper. The 8 nm NCs showed the highest FE of 90% toward CO at −0.67 $V_{RHE}$ (0.5 M KHCO₃, pH = 7.3) (Figure 3A−C). While producing more hydrogen, the smaller particles had the highest activity (current density expressed as A/g) at all the different potentials (Figure 3D). By approximating the spherical Au NCs to perfect cuboctahedra,

one can plot the density of adsorption sites (corner and edge) as a function of the size. Considering the superior catalytic activity of edges toward CO, it was concluded that the 8 nm particles exhibited the maximum FE because they provide a near-optimum number of edge sites (coordination number = 7) while minimizing corner sites (coordination number = 5) which are selective for HER. As the diameter increases, the reactivity of the particles becomes dominated by the (111) facets which require a higher energy for the formation of key intermediate COOH* compared with the stepped (211) surfaces.

In a follow up study, the same authors showed that ultrathin Au NWs had higher activity than the NCs as a result of the higher ratio between edge/corner atoms on the surface (Figure 4).[48] In this study, the effect of NW length (500, 100, and 15 nm) was tested, and here the ligands were removed by treatment with acetic acid while the electrode preparation was the same as the previous report on Au NCs. The authors reported that 500 nm Au NWs exhibited the best performance with 94% FE toward CO at −0.35 $V_{RHE}$ and also their intrinsic activity (1.84 A/g) was much higher than polycrystalline gold. Again, calculations suggested that both COOH* and CO* preferentially bind to the bridge site on the Au NW edge with COOH* binding marginally stronger than that on the Au (211) edge but CO* binding marginally weaker than that on Au₁₃ clusters. Basically, the NW surfaces possessed the optimum configuration to activate CO₂ to COOH* yet facilitated the CO desorption. Testing over 12 h showed the formation of small gold particles with a decreased activity for the CO formation. These two examples together underline the importance of stabilizing the key intermediate COOH* at a favorable binding site, i.e., the edge site in the case of Au NCs, for efficient and selective electrocatalytic reduction of CO₂ to CO.

*Copper NCs.* Manthiram et al. have synthesized 7.0 ± 0.4 nm spherical Cu NCs and demonstrated an increased FE toward methane compared with copper foil (76% vs 44% at −1.35 $V_{RHE}$ in 0.1 M NaHCO₃ buffer, pH = 6.8).[49] Herein, the NCs were simply deposited on glassy carbon without addition of carbon particles or binders. The increased methane production was explained by invoking the exposure of active sites such as (210) planes when the NCs were isolated from each other, thus at low catalyst loading. These sites were lost in continuous films as the NCs got in closer proximity to one another. Based on the Tafel slope analysis (log(current density) vs applied potential) the authors proposed that the first electron transfer step to form $CO_2^{\bullet-}$ from CO₂, before the formation of COOH*, was promoted on the NC surface. However, probably due to the different catalyst loadings, this result contrasts with our work, the work from Yang, and the work from Strasser, where mostly hydrogen was produced by spherical Cu NCs of around 10 nm or so, independent of the ligands or synthesis method.[50−52]

The group led by Yang studied ultrathin fivefold twinned copper NWs, loaded on carbon black and deposited on glassy carbon, which reached a maximum FE of 55% toward methane, 5% of different carbon products, and the rest hydrogen (at −1.25 $V_{RHE}$ in 0.1 M KHCO₃). Such a selectivity was attributed by the authors to low-coordinated edge sites.[53]

From single crystal studies, the (100) surface is known to promote the formation of ethylene over methane.[54,55] One work led by Nilsson has shown that copper nanocubes grown electrochemically from copper foil decrease the onset potential
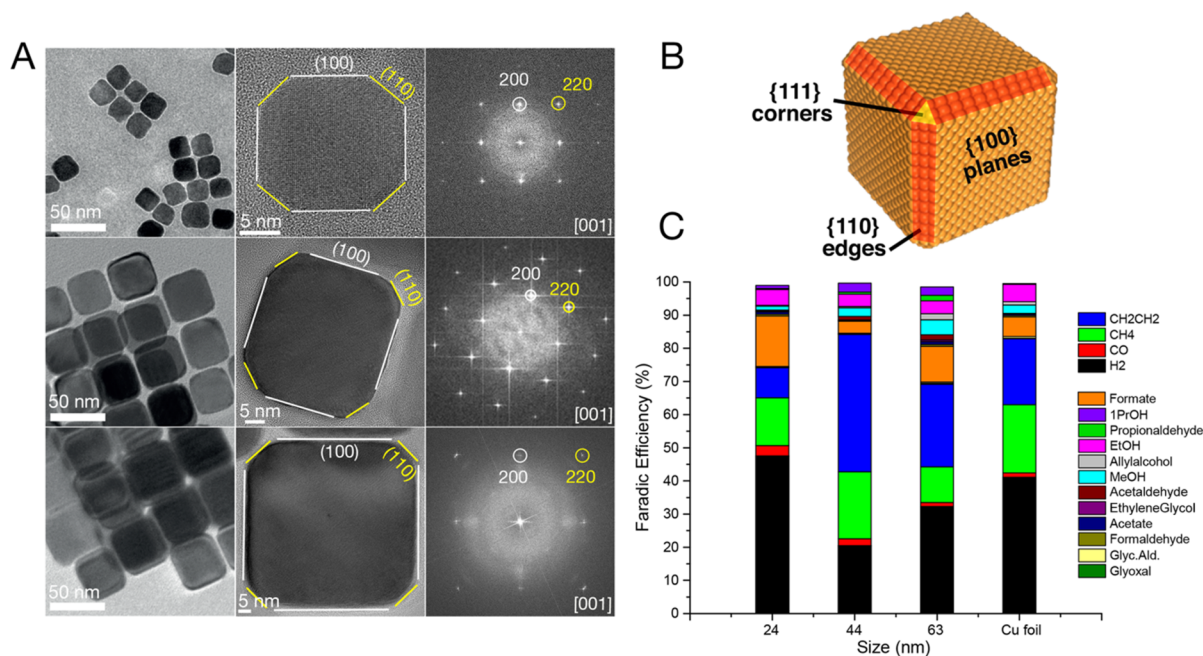
**Figure 5.** Size-dependent electrocatalytic behavior of Cu nanocubes. (A) TEM images of Cu cubes with an average edge lengths of 24, 44, and 63 nm and HRTEM images and the corresponding fast Fourier transform (FFT) patterns of Cu cubes with an approximate edge length of 16, 41, and 65 nm. (B) Schematic model of a truncated cube comprising {100}, {110}, and {111} planes. (C) Bar graph reporting the FE for each product in the different sizes of Cu cubes and in the Cu foil at $-1.1$ $V_{RHE}$. The figures in the left column of (A) and the graph in (C) are adapted both with permission from ref 50. Copyright 2016 Wiley-VCH Verlag GmbH & Co. The figures in the middle and right column of (A) are adapted with permission from ref 57. Copyright 2018 Nature Publishing Group.
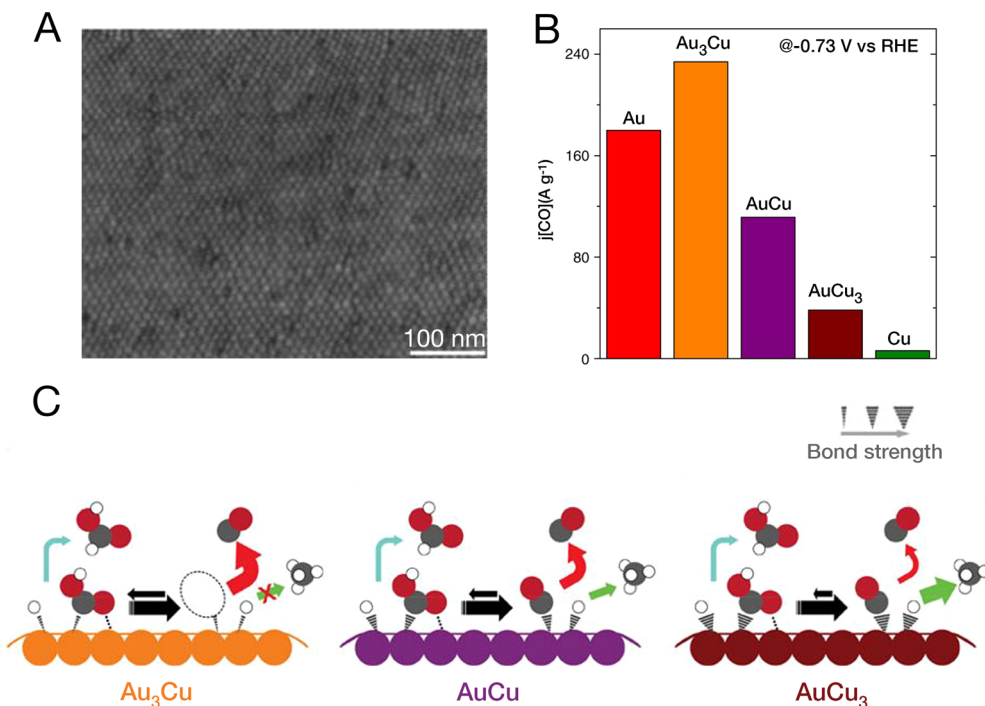


**Figure 6.** Alloyed AuCu NCs with varied Au/Cu ratios for $CO_2RR$. (A) Scanning electron microscopy (SEM) image of an $AuCu_3$ NC monolayer transferred to a substrate using the Langmuir−Schaefer technique. (B) CO mass activity of the Au−Cu bimetallic NCs at $-0.73$ $V_{RHE}$. Mass activity is based on the overall mass of Au and Cu. (C) Schematic showing the proposed mechanism for $CO_2$ reduction on the catalyst surface of Au−Cu bimetallic NCs. Gray filled circles are C, red are O, and white are H. The relative intermediate binding strength is indicated by the stroke weight (on the top right corner). Additional binding between the COOH and the catalyst surface is presented as a dotted line. Arrows between the adsorbed COOH and adsorbed CO are to show the difference in probability of having COOH adsorbed on different types of surfaces. Colored arrows indicate the pathway to each product: red for CO, blue for formate, and green for hydrocarbons. Larger arrows indicate higher turnover. Adapted with permission from ref 51. Copyright 2014 Nature Publishing Group.

for ethylene prodution.[56] Our group has contributed to this topic by synthesizing Cu nanocubes with tunable sizes including 24, 44, and 63 nm (Figure 5A,B).[50,57] The electrodes were prepared by simply spin-coating the NCs on a glassy carbon plate to exclude any possible interference of binders on the intrinsic activity. The interesting result was, once again, the nonlinear dependence between the size and FE toward ethylene with the 44 nm cubes exhibiting a total 80% FE toward $CO_2RR$ and 41% FE toward ethylene (Figure 5C). As shown by high resolution TEM analysis, in addition to {100} facets, each cube exhibits {110} edges and {111} corners (Figure 5A,B). The latter do not impact substantially the catalytic behavior considering that Cu {111} is supposed to generate methane, which is not the main product from the cubes. Based on initial theory results and on degradation studies which are to be described later, we believe that the catalytic sites favoring C–C coupling reside at the intersection between the {110} and the {100} facets. As the size of the cubes increases, the ratio {110}/{100} decreases, and the 44 nm cubes possess the near optimal ratio for maximizing the limiting step for the ethylene production.

*Bimetallic NCs.* While different examples of bimetallic electrocatalysts have been reported in the literature, here we focus only on those employing NCs prepared by colloidal methods. CuAu bimetallic NCs have been studied as a platform to investigate the compositional effect on their selectivity toward CO.[51] Colloidal chemistry can tune the composition in a broad range while keeping the other parameters, such as the size and the shape, constant. Hence, highly monodisperse 10 nm spherical NCs were synthesized with the composition ranging from Au, $Au_3Cu$, AuCu, and $AuCu_3$ to Cu and assembled as a monolayer on glassy carbon (Figure 6A). When tested in 0.1 M $KHCO_3$ at pH = 6.8, 10 nm Au NCs produce CO and $H_2$ and spherical Cu NCs mostly hydrogen, similarly to previous studies.[50,52] When comparing the different compositions at the lowest potential ($-0.73$ $V_{RHE}$), interestingly, $Au_3Cu$ is the catalyst with the highest activity toward CO (Figure 6B). Based on purely electronic effects, Au is expected to perform more efficiently than the alloys. The obtained result was then explained by invoking a synergistic effect between electronic and geometric effects leading to breaking the scaling relations to stabilize the COOH intermediate in $Au_3Cu$ (Figure 6C).

In this study, the authors suggested a homogeneous distribution of the two metals within the alloyed AuCu NCs. The same group explored the effect of structural order focusing on Au/Cu atomic ratio = 1/1.[58] It was found that the disorder (face-centered cubic)/order (face-centered tetragonal) transition transformed AuCu from an inert to a very active catalyst for converting $CO_2$ to CO (Figure 7). In particular the ordered-AuCu NCs were more active than the corresponding Au NCs, reflected by the higher CO partial current density, which however still preserved the highest FE toward CO. The degree of atomic ordering was assessed by different techniques spanning from X-ray diffractometry (XRD) to aberration-corrected high-angle annular dark-field scanning transmission electron microscopy (HAADF-STEM) and X-ray absorption spectroscopy. While investigating the transition from a disordered to an ordered atomic arrangement, the authors discovered that it is actually accompanied by the formation of a three-atoms-thick gold overlayer. Thermochemical density functional theory (DFT) calculations showed that $CO_2$ conversion was favored over $H_2$ evolution in the ordered
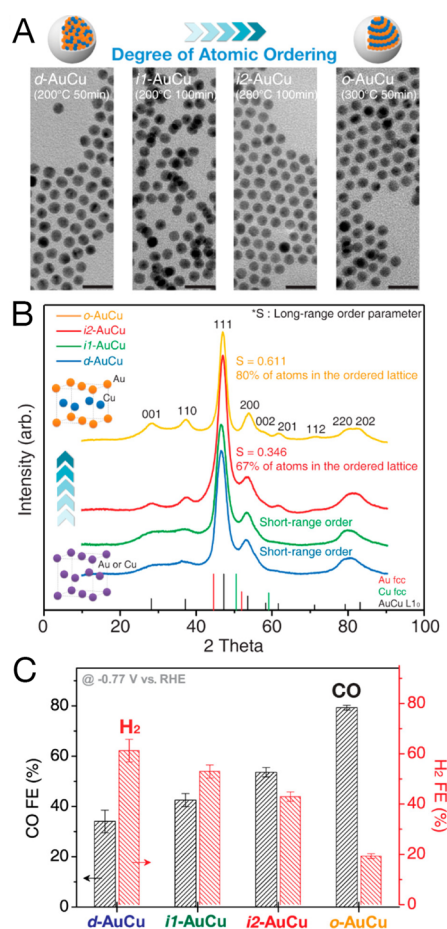


**Figure 7.** AuCu bimetallic NCs with varied atomic ordering for $CO_2RR$. (A) TEM images of AuCu bimetallic NCs synthesized at various conditions allowing for systematic tuning of the degree of ordering. Scale bar, 20 nm. (B) XRD of AuCu bimetallic NCs. (C) Electrochemical $CO_2$ reduction activities of AuCu bimetallic NCs evaluated by FE of CO and $H_2$. Measurements were conducted at $-0.77$ $V_{RHE}$ with 0.1 M $KHCO_3$ solution (pH = 6.8) at 1 atm $CO_2$ and room temperature. Reprinted with permission from ref 58. Copyright 2017 American Chemical Society.

system as a result of a 6% compressive strain arising in the gold overlayer. While considered negligible, electronic effects were also not fully excluded considering a theoretical shift in the d-band center between disordered-AuCu and ordered-AuCu, the latter being much closer to pure Au. DFT calculations suggested that the gold layer underwent compressive straining and that such structural modification combined with the shift in the d-band center for the AuCu ordered NCs accounted for the observed electrochemical behavior.

One second example of bimetallic NCs for $CO_2RR$ concerns core@shell Pd@Cu NCs from the group led by Yin (Figure 8).[59] Here, they were able to achieve surface enrichment of high energy Cu (110) facets by using Pd as seeds and through selective etching with selenium dissolved in trioctylphosphine. When tested as electrocatalysts, the rhombic dodecahedrons exhibited higher activity and selectivity toward $CO_2RR$ compared with other shapes, most likely due to the exposure of high energy surfaces with high coordination number. Unlike in previous cases, it is unclear whether the second metal, Pd, being deeply in the core, participates in the $CO_2RR$ which is a surface reaction.
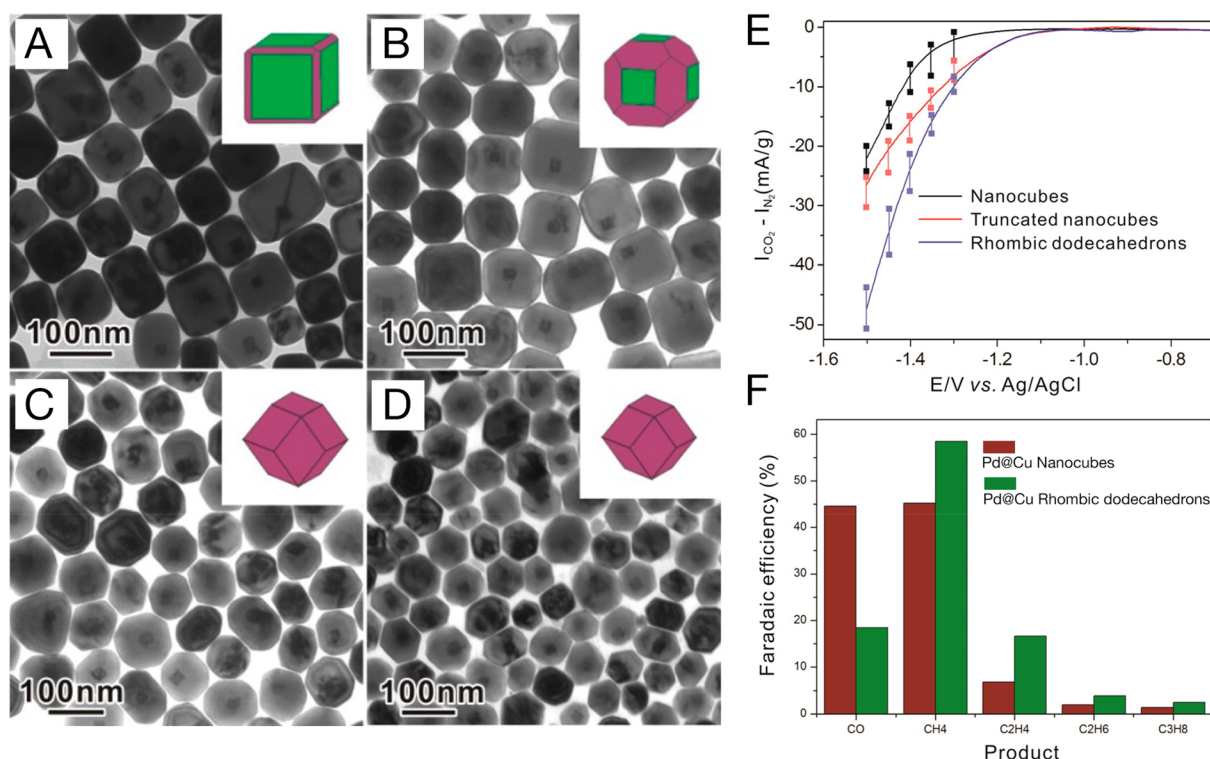
**Figure 8.** Core@shell Pd@Cu NCs with high-energy facets for $CO_2RR$. (A–D) TEM images of as-etched Cu NCs subjected to different periods of etching: (A) 4 h, (B) 8 h, (C) 12 h, and (D) 24 h. (E) $CO_2$ electroreduction currents corrected for currents in $CO_2$-free solutions for Cu NCs with different shapes: nanocubes, truncated nanocubes, and rhombic dodecahedrons. The electrochemical evaluation was conducted in a solution containing 0.25 M $K_2CO_3$ at a sweep rate of 20 mV $s^{-1}$. (F) Comparison of the FE between Cu nanocubes and Cu rhombic dodecahedrons toward $CO_2$ electroreduction. Adapted with permission from ref 59. Copyright 2016 American Chemical Society.

*Doped NCs.* Doping, whether intrinsic or extrinsic, contributes to such changes of electronic structure and,thus, it is expected to modify the catalytic activity. Recently, the group led by Sargent showed that $Cu_2S$ core with a vacancy-rich copper shell (CSVE-Cu) NCs, fabricated by partially reducing colloidal vacancy-enriched $Cu_2S$ NCs, modulates the reaction pathway at the branching point between ethylene and ethanol to favor the production of alcohols (Figure 9A).[37] DFT suggested that subsurface sulfur atoms and copper vacancy defects synergistically increased the barrier to the ethylene pathway. At −0.95 $V_{RHE}$ the alcohol-to-ethylene ratio was enhanced from 0.18 on the bare Cu NCs to 1.2 on the engineered catalyst, though the overall FE for $C_{2+}$ products remained similar. This indicated that the Faradaic current was shifted from producing ethylene to producing alcohols. After evaluating the intrinsic activity and selectivity under the most common conditions (NCs deposited on glassy carbon and in a conventional liquid cell with a 0.1 M $KHCO_3$ electrolyte), the engineered catalyst was tested in an ad hoc designed reactor (Figure 9B). Herein, the NCs were spray coated on a carbon gas diffusion layer, so to overcome the solubility limit of $CO_2$ in water, and the electrolyte was 1 M KOH. The $OH^-$ is supposed to affect the bound O* intermediates of the ethylene pathway but to leave the ethanol pathway unchanged.[38] The engineered catalyst exhibited the lower overpotential (Figure 9C). When operating at current densities in the range 200–600 mA/$cm^2$, which gets closer to the values for an industrially relevant electrolyzer, up to 32% FE for alcohol was reached (Figure 9D) and the overall performance overcame control catalysts and state of the art (Figure 9E). This work clearly highlights the importance of combining catalyst design with

reactor engineering and electrolyte tuning in order to move toward industrially relevant targets.

**3.2. Identification of Degradation Pathways.** Well-defined and monodispersed colloidal NCs can aid to elucidate morphological changes and deactivation mechanisms during catalysis.[60,61] A few studies along this direction have also been conducted in $CO_2RR$.[49,57,62,63] In their study on the 8 nm Cu NCs, Manthiram et al. showed an increase in particle size during electrolysis up to 23 ± 8 nm even in the absence of $CO_2$, highlighting that catalyst morphological changes will most likely occur under the high negative potential applied during the reaction.[49] The same authors studied the dendritic assembly of dodecanethiol-capped 4 nm gold NCs under electrochemical $CO_2RR$ conditions (−1.2 $V_{RHE}$ in 0.1 M $NaHCO_3$ buffer, pH = 6.8) on glassy carbon as a support (Figure 10A).[62] In this aggregation process, the native thiol ligands on the surface of the gold NCs were suggested to play a key role based on a solubility argument. At the negative applied potential, the ligands electro-desorbed from the surface. However, at acidic pH they are protonated and remained physiosorbed on the surface; thus, dendritic assembly did not occur. At basic pH the thiol is not protonated, and thus it is soluble in the water electrolyte, which implied that dendritic assembly occurred. Dendritic assembly occurred also at neutral pH contrary to what was expected based on the $pK_a$ of the dodecanthiol (10.5). Under reductive polarization the electrolyte could become quite more basic in the vicinity of the electrode, especially in electrolytes with low buffer capacity. Indeed in 0.5 M $NaHCO_3$ buffer, a reduced dendritic assembly was observed. Additionally, the increased ionic strength might contribute to screening charge−charge repulsion between the
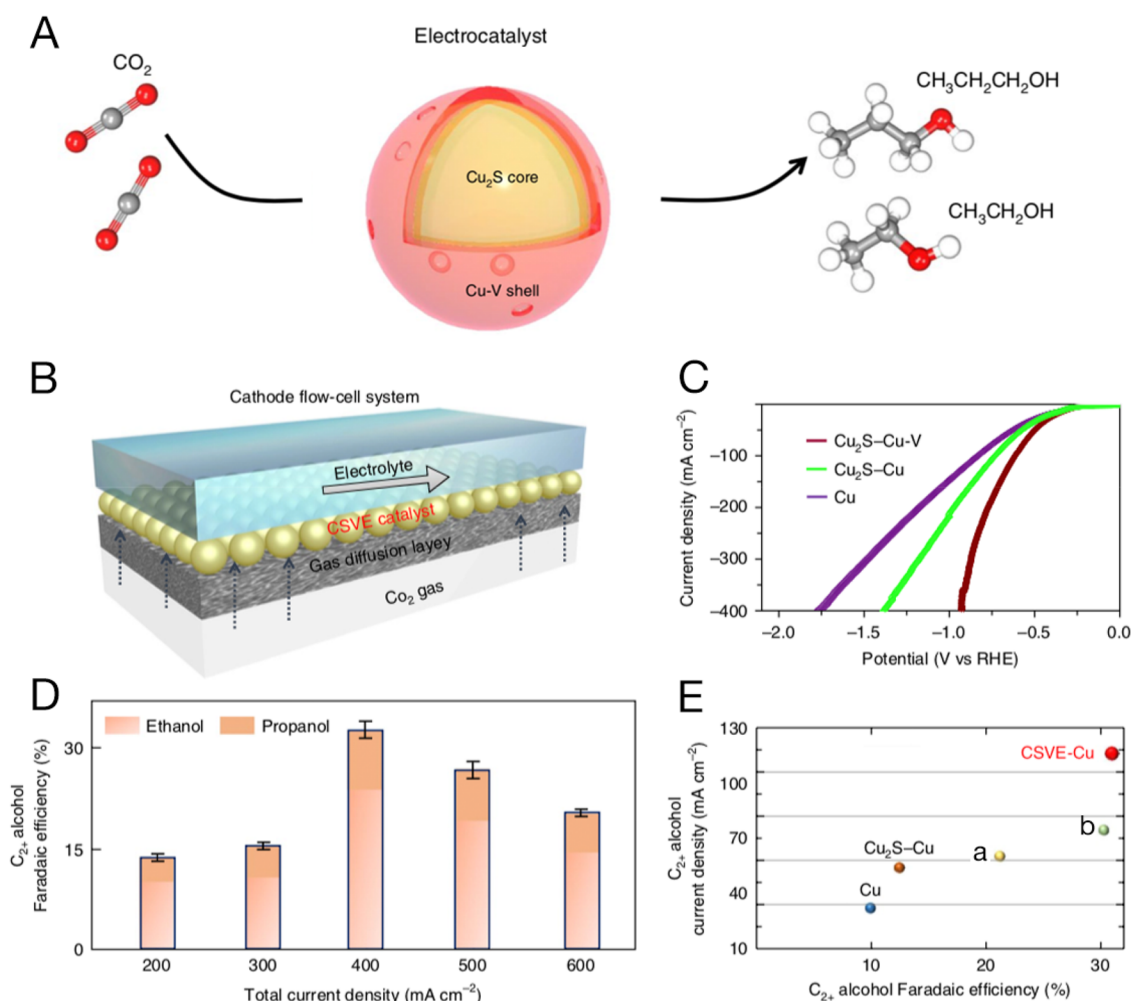
**Figure 9.** Cu$_2$S core with vacancy-rich Cu shell (CSVE-Cu) NCs for CO$_2$RR. (A) Schematic illustration of Cu$_2$S−Cu−V electrocatalyst design for production of multicarbon alcohols from CO$_2$ reduction. (B) Schematic illustration of the cathode flow-cell system using a gas-diffusion electrode for CO$_2$. (C) Linear sweep voltammetry curves in the 1 M KOH electrolyte for the Cu$_2$S−Cu−V and control catalysts. (D) FE of C$_{2+}$ alcohols (ethanol and propanol) on Cu$_2$S−Cu−V nanocatalyst in the current density range 200−600 mA cm$^{-2}$. (E) Plot of C$_{2+}$ alcohol partial current density versus maximum C$_{2+}$ alcohol FE for catalysts in a flow-cell system (compared with those from Xie et al. *Nat. Commun.* **2016**, 7, 12697 and Sargent et al. *ACS Catal.* **2016**, 6, 8115). Adapted with permission from ref 37. Copyright 2018 Nature Publishing Group.

physiosorbed thiolates, inhibiting their dissociation from the surface. Dielectric screening might also play a role considering that dendritic assembly was suppressed going from 0.1 to 0.5 M KOH. Solubility arguments were supported also by the fact that the dodecanthiol was better in suppressing dendritic assembly relative to dodecylamine. Interestingly, the dendritic assembly occurred also in the presence of binders, suggesting that an actual bond with the substrate surface might be needed to avoid the (dendritic) aggregation.

The group led by Yang reported a very rapid evolution (within 7 min) of 7 nm Cu spheres into cube-like particles (10−40 nm) when they were densely packed at a very high loading on carbon paper (Figure 10B),[63] a phenomenon that we also observed in our experiments with similar samples. Concomitant to this morphological change, a significant decrease of HER and increase of CO$_2$RR was observed with higher selectivity toward C$_2$−C$_3$ products at a relatively low overpotential compared with other studies on Cu nanocubes (FE$_{C2-C3}$ = 49% @ −0.81 V$_{RHE}$ in 0.1 M KHCO$_3$). Because the sole morphological features cannot explain the increased selectivity, two hypotheses were proposed and left open: (1) a unique restructuring of the {100}surface toward novel active

sites occurs during electrochemistry; (2) the mixture of cube-like together with smaller particles is the unique feature behind the catalytic behavior.

Driven by the same interest to monitor morphological changes of the catalysts during CO$_2$RR, we have recently studied different metallic electrocatalysts over the course of 12 h.[57] While focusing on Cu nanocubes of different sizes, Ag and Pd were also tested. By exploring many different parameters, we discovered a unique and general degradation mechanism which is the potential-driven nanoclustering, and it is illustrated in Figure 10C. Grand potential DFT helped us to predict the equilibrium shape of Cu nanoparticles with H- and CO- adsorbates and confirmed the negative potential to be the main driving force for the degradation. The degradation started at the {110}/{100}intersections in agreement with the hypothesis of these being the active sites for ethylene production. The clusters are metallic copper, though it remains to be elucidated which are the actual chemical species first detaching from the surface. As the clustering proceeded, HER increased and CO$_2$RR decreased. Interestingly, while Ag nanocubes underwent clustering under the same conditions as those applied for copper (i.e., −1.1 V$_{RHE}$, 0.1 M KHCO$_3$),
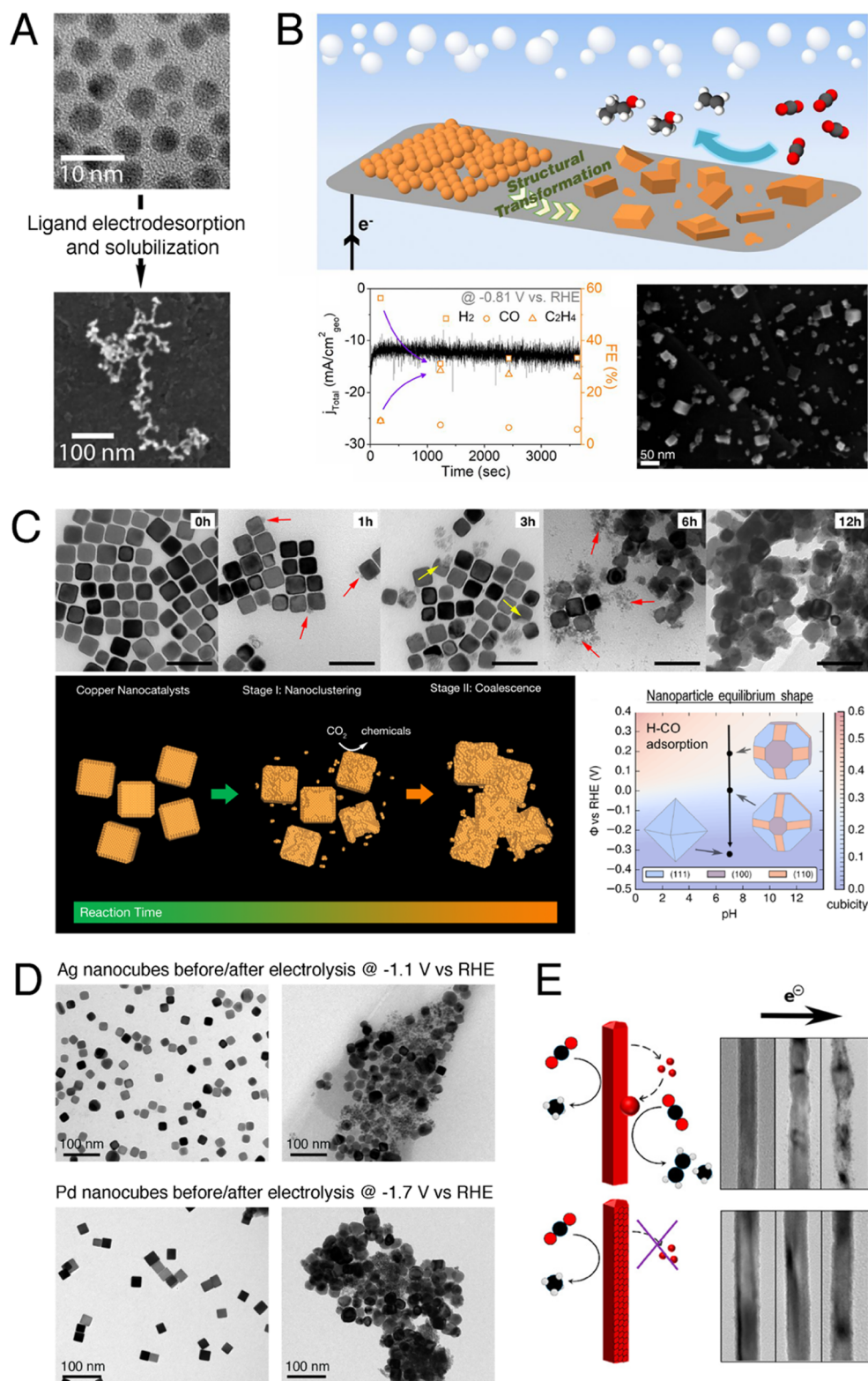
**Figure 10.** Morphological transformations of NC catalysts under CO$_2$RR conditions. (A) Dendritic assembly of Au NCs upon electrodesorption of the organic ligands. (B) Structural transformation of Cu NC ensembles to an active catalyst for C$_2$–C$_3$ product formation. (C) Potential driven nanoclustering of Cu nanocubes and the predicted equilibrium shapes of Cu nanoparticles with H- and CO-adsorbates at different potentials. (D) Potential driven nanoclustering of Ag and Pd nanocubes under −1.1 and −1.7 V vs RHE, respectively. (E) Nanoclustering occurring in Cu NWs and being suppressed after the wires are wrapped with graphene oxide. The figure in (A) is adapted with permission from ref 62. Copyright 2014 American Chemical Society. The figure in (B) is reprinted with permission from ref 63. Copyright 2017 National Academy of Sciences. The figures in (C) and (D) are adapted with permission from ref 57, licensed under a Creative Commons Attribution 4.0 International License http://creativecommons.org/licenses/by/4.0/. Copyright 2018 Nature Publishing Group. The figure in (E) is reprinted with permission from ref 53. Copyright 2017 American Chemical Society.

Pd nanocubes required a much more negative potential ($-1.7$ $V_{RHE}$, 0.1 M $KHCO_3$) (Figure 10D). This behavior might be due to the higher cohesive energy of Pd compared to Cu and Ag.[64] Regarding the role played by the ligands, we did find that they electrodesorbed during the first hour or so. Their removal prior to the electrochemical testing resulted only in faster degradation kinetics but did not impact the degradation pathway itself. After revealing that nanoclustering is mainly induced by the negative potential, two mitigation strategies come into mind. From a practical perspective, wrapping the catalysts with a thin, porous, and conductive material can offer a good solution by physically impeding the detachment of clusters from the catalyst while still preserving the necessary conductivity and $CO_2$ accessibility to the active sites. Actually, the group led by Yang in the work on Cu NWs described above observed nanoclustering as well, and they were able to prevent it by wrapping the NWs with graphene oxide (Figure 10E).[53] From a mechanistic perspective, it motivates future research involving the introduction of suitable promoters (metal oxides, ligands, or another metal) that change the metal cohesive energy or that can reduce the overpotential of Cu electrocatalysts toward $CO_2RR$ through mutual interactions at the catalyst–promoter interface.

**3.3. Role of the Organic Ligands.** Organic ligands are crucial for the control of the composition and of the morphology of colloidal NCs as they play the double role of tuning the precursor reactivity and of modulating the NC surface energy. In most cases, when NCs are used as heterogeneous catalysts, the organic ligands are removed in order to access the intrinsic reactivity of the clean surfaces. To this aim, different strategies are available, spanning from annealing in different atmospheres and plasma treatments to solvent washing and electrochemical desorption.[44,65−69] To preserve the synthetic efforts, it is mandatory to carefully check that no changes occur in the catalysts after these treatments. Spherical metallic NCs anchored on a metal oxide support are most likely to retain their size, shape, and composition compared to faceted alloyed nanoparticles deposited on smooth glassy carbon, which is the most common substrate used so far for electrochemical $CO_2RR$. The latter are kinetic products which will evolve into the thermodynamically stable ones (i.e., faceted NCs into spherical NCs, alloys into phase segregated metallic domains) upon annealing, especially considering the lack of chemical interaction with the carbon support underneath. We have found nitrogen plasma to be a good treatment for ligand removal from the surface of the Cu nanocubes, which sinter with even a mild thermal annealing (Figure 11A−C). Nitrogen plasma is not ideal because it leaves carbon residues from ligand decomposition behind (Figure 11D), yet it is preferable to oxygen plasma which oxidizes the surface of the Cu nanocubes. In studies wherein the basic fundamental understanding of structure/property relations is achieved through comparison across samples, ligand removal might not be needed if one assures that the nature of the ligands and their mass fraction stay similar in each sample. This approach was undertaken by our group and by Yang's group in the study of AuCu NCs: "Any thermal or chemical treatments were avoided so as not to alter their inherent structure produced."[50,58] If the native ligands are conserved, their fate during electrochemistry must be monitored as they will most likely be electro-desorbed under the $CO_2RR$ conditions.[57,62]
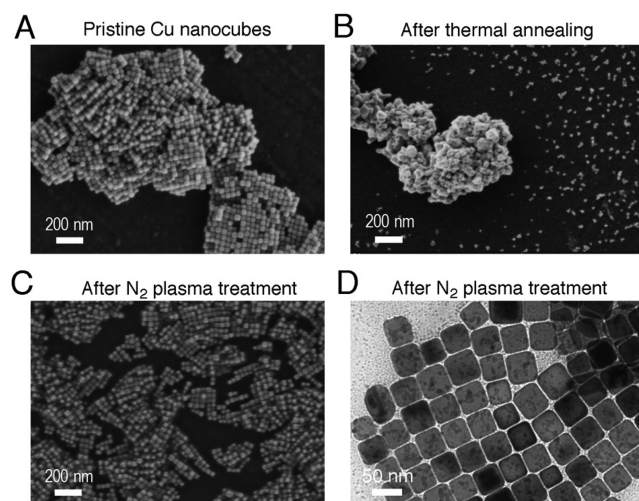
**Figure 11.** Treatments for ligand removal from Cu nanocubes. (A−C) SEM images of (A) pristine, (B) thermally annealed (100 °C for 1 h), and (C) $N_2$-plasma treated Cu nanocubes (plasma power 80 W for 90 s) on glassy carbon substrate. (D) TEM images of $N_2$-plasma treated Cu nanocubes with carbon debris from decomposed ligands. Adapted with permission from ref 57, licensed under a Creative Commons Attribution 4.0 International License http://creativecommons.org/licenses/by/4.0/. Copyright 2018 Nature Publishing Group.

## 4. OUTLOOK

Precisely engineered colloidal NCs are undoubtfully great model systems to identify relationships between size/structure/composition and activity/selectivity/stability in electrocatalytic $CO_2RR$. The systematic variation of their size often reveals unexpected trends which lead to performance optimization. Faceted nanocrystals serve the purpose to translate single crystal studies to more realistic conditions, including the use of gas diffusion electrodes. Furthermore, electronic and geometric effects might intervene at nanoscale interfaces between two facets to generate new catalytic motifs which stabilize certain intermediates and direct selectivity. While this facet-dependent reactivity adds new degrees of freedom in the 2D activity map shown in Figure 1C, which is calculated for bulk metallic surfaces, modifying the size and shape of monometallic NC catalysts is not enough to reach the top of the volcano. Domains of different chemical natures are indeed needed to break the scaling relationships.

Compared with other synthetic techniques commonly used for the preparation of catalysts (i.e., coprecipitation, impregnation, thermal decomposition), colloidal chemistry offers the unique capability to access metastable phases and compositions as well as to precisely control the nature and the extent of interfaces between different domains. Some studies have been pursued, such as the one on CuAu cited above, yet much more can be done to further exploit such a synthetic tunability, for example, by synthesizing metastable multinary alloys or nanocrystalline heterostructures including metal and metal oxide domains or interfacing nanocrystals with polymers and metal organic frameworks. Furthermore, one might look into strategies to confer functionality to the organic ligands by properly engineering the anchoring groups, so to prevent electro-desorption, and the aliphatic chain so to interact with $CO_2$ and/or with key reaction intermediates such as CO* and CHO*. Being able to design ligands which confer stability

while aiding selectivity without compromising activity would represent big progress in the field.

Because of their intrinsic monodispersity and uniformity, colloidal NCs are ideal systems to study degradation mechanisms to guide the development of the proper mitigation strategies. Considering that the most active sites will most likely be the fastest ones degrading, these studies might aid the identification of the active sites as well. Looking at the future, in situ/operando techniques, including X-ray spectroscopies and TEM, will be invaluable to correlate the structural and compositional changes to the electrocatalytic behavior. While being a very powerful and promising technique, operando liquid TEM comes with its challenges.[70] Great care must be taken in the fabrication of the chip used for the liquid cell to ensure resolution while reproducing the actual reaction conditions, having in mind that side reactions might occur due to radical formation under the electron beam. As the field moves toward this direction, carefully conducted identical location experiments will be crucial.[67,70]

Today the advantage of using colloidal NCs as model systems in $CO_2RR$ as well as in other electrocatalytic reactions is undoubtful. A few examples show that coupling catalyst design and reactor engineering can get us closer to the targets for an industrially relevant $CO_2$ electrolyzer.[37,38] The rising of companies like Nanosys, UbiQD, and QDVision, which utilize colloidal NCs in displays and sensors, evidence that these man-made nanomaterials can offer actual technological solutions when compelling and/or competitive properties are discovered. Hence, the idea of a commercial $CO_2RR$ electrolyzer incorporating colloidal NC catalysts might become a reality in the future.

## ■ AUTHOR INFORMATION

**Corresponding Author**
*(R.B.) E-mail: raffaella.buonsanti@epfl.ch.
**ORCID** ⊙
Raffaella Buonsanti: 0000-0002-6592-1869
**Notes**
The authors declare no competing financial interest.

**Biographies**

Jianfeng Huang has been a postdoctoral fellow with Prof. Raffaella Buonsanti at École Polytechnique Fédérale de Lausanne (EPFL) since May 2016. He received his Ph.D. degree in chemical sciences under the supervision of Prof. Yu Han at King Abdullah University of Science and Technology (KAUST) in December 2015. His research is mainly focused on engineering colloidal nanocrystals for energy-related applications.

Raffaella Buonsanti has been a tenure-track Assistant Professor in the Institute of Chemical Sciences and Engineering at EPFL since October 2015. She graduated in Nanochemistry at the National Nanotechnology Laboratory, University of Salento (Italy, 2006-2010, with Prof. Davide Cozzoli) followed by a postdoc at the Molecular Foundry, Lawrence Berkeley National Laboratory (United States, 2010−2012, with Prof. Delia Milliron). After one year as a project scientist in the same institution (United States, 2012−2013), Raffaella was a tenure-track Staff Scientist in the Department of Materials Science within the Joint Center for Artificial Photosynthesis at Lawrence Berkeley National Laboratory (United States, 2013−2015), before moving to EPFL. Here, through her core expertise in colloidal synthesis, she develops novel approaches to complex materials to drive chemical transformations, with particular emphasis on energy-related reactions such as $CO_2$ reduction and water oxidation.

## ■ REFERENCES

(1) Lim, X. How to make the most of carbon dioxide. *Nature* **2015**, *526*, 628−630.

(2) Kuhl, K. P.; Cave, E. R.; Abram, D. N.; Jaramillo, T. F. New insights into the electrochemical reduction of carbon dioxide on metallic copper surfaces. *Energy Environ. Sci.* **2012**, *5*, 7050−7059.

(3) Hori, Y.; Murata, A.; Takahashi, R. Formation of Hydrocarbons in the Electrochemical Reduction of Carbon-Dioxide at a Copper Electrode in Aqueous-Solution. *J. Chem. Soc., Faraday Trans. 1* **1989**, *85*, 2309−2326.

(4) Kuhl, K. P.; Hatsukade, T.; Cave, E. R.; Abram, D. N.; Kibsgaard, J.; Jaramillo, T. F. Electrocatalytic conversion of carbon dioxide to methane and methanol on transition metal surfaces. *J. Am. Chem. Soc.* **2014**, *136*, 14107−14113.

(5) Schouten, K. J. P.; Kwon, Y.; van der Ham, C. J. M.; Qin, Z.; Koper, M. T. M. A new mechanism for the selectivity to C1 and C2 species in the electrochemical reduction of carbon dioxide on copper electrodes. *Chem. Sci.* **2011**, *2*, 1902−1909.

(6) Liu, X.; Xiao, J.; Peng, H.; Hong, X.; Chan, K.; Norskov, J. K. Understanding trends in electrochemical carbon dioxide reduction rates. *Nat. Commun.* **2017**, *8*, 15438.

(7) Peterson, A. A.; Abild-Pedersen, F.; Studt, F.; Rossmeisl, J.; Nørskov, J. K. How copper catalyzes the electroreduction of carbon dioxide into hydrocarbon fuels. *Energy Environ. Sci.* **2010**, *3*, 1311−1315.

(8) Montoya, J. H.; Shi, C.; Chan, K.; Norskov, J. K. Theoretical Insights into a CO Dimerization Mechanism in CO2 Electro-reduction. *J. Phys. Chem. Lett.* **2015**, *6*, 2032−2037.

(9) Kortlever, R.; Shen, J.; Schouten, K. J.; Calle-Vallejo, F.; Koper, M. T. Catalysts and Reaction Pathways for the Electrochemical Reduction of Carbon Dioxide. *J. Phys. Chem. Lett.* **2015**, *6*, 4073−4082.

(10) Garza, A. J.; Bell, A. T.; Head-Gordon, M. Mechanism of CO2 Reduction at Copper Surfaces: Pathways to C2 Products. *ACS Catal.* **2018**, *8*, 1490−1499.

(11) Schreier, M.; Yoon, Y.; Jackson, M. N.; Surendranath, Y. Competition between H and CO for Active Sites Governs Copper-Mediated Electrosynthesis of Hydrocarbon Fuels. *Angew. Chem., Int. Ed.* **2018**, *57*, 10221−10225.

(12) Wuttig, A.; Yaguchi, M.; Motobayashi, K.; Osawa, M.; Surendranath, Y. Inhibited proton transfer enhances Au-catalyzed CO2-to-fuels selectivity. *Proc. Natl. Acad. Sci. U. S. A.* **2016**, *113*, E4585−4593.

(13) Yoon, Y.; Hall, A. S.; Surendranath, Y. Tuning of Silver Catalyst Mesostructure Promotes Selective Carbon Dioxide Conversion into Fuels. *Angew. Chem., Int. Ed.* **2016**, *55*, 15282−15286.

(14) Lobaccaro, P.; Singh, M. R.; Clark, E. L.; Kwon, Y.; Bell, A. T.; Ager, J. W. Effects of temperature and gas-liquid mass transfer on the operation of small electrochemical cells for the quantitative evaluation of CO2 reduction electrocatalysts. *Phys. Chem. Chem. Phys.* **2016**, *18*, 26777−26785.

(15) Hori, Y.; Takahashi, R.; Yoshinami, Y.; Murata, A. Electrochemical Reduction of CO at a Copper Electrode. *J. Phys. Chem. B* **1997**, *101*, 7075−7081.

(16) Schouten, K. J. P.; Pérez Gallent, E.; Koper, M. T. M. The influence of pH on the reduction of CO and CO2 to hydrocarbons on copper electrodes. *J. Electroanal. Chem.* **2014**, *716*, 53−57.

(17) Dunwell, M.; Lu, Q.; Heyes, J. M.; Rosen, J.; Chen, J. G.; Yan, Y.; Jiao, F.; Xu, B. The Central Role of Bicarbonate in the Electrochemical Reduction of Carbon Dioxide on Gold. *J. Am. Chem. Soc.* **2017**, *139*, 3774−3783.

(18) Ogura, K.; Ferrell, J. R.; Cugini, A. V.; Smotkin, E. S.; Salazar-Villalpando, M. D. CO2 attraction by specifically adsorbed anions and subsequent accelerated electrochemical reduction. *Electrochim. Acta* **2010**, *56*, 381−386.

(19) Sandberg, R. B.; Montoya, J. H.; Chan, K.; Nørskov, J. K. CO-CO coupling on Cu facets: Coverage, strain and field effects. *Surf. Sci.* **2016**, *654*, 56−62.

(20) Chen, L. D.; Urushihara, M.; Chan, K.; Nørskov, J. K. Electric Field Effects in Electrochemical CO2 Reduction. *ACS Catal.* **2016**, *6*, 7133−7139.

(21) Liu, M.; Pang, Y. J.; Zhang, B.; De Luna, P.; Voznyy, O.; Xu, J. X.; Zheng, X. L.; Dinh, C. T.; Fan, F. J.; Cao, C. H.; de Arquer, F. P. G.; Safaei, T. S.; Mepham, A.; Klinkova, A.; Kumacheva, E.; Filleter, T.; Sinton, D.; Kelley, S. O.; Sargent, E. H. Enhanced electrocatalytic CO2 reduction via field-induced reagent concentration. *Nature* **2016**, *537*, 382−386.

(22) Singh, M. R.; Kwon, Y.; Lum, Y.; Ager, J. W.; Bell, A. T. Hydrolysis of Electrolyte Cations Enhances the Electrochemical Reduction of CO2 over Ag and Cu. *J. Am. Chem. Soc.* **2016**, *138*, 13006−13012.

(23) Akhade, S. A.; McCrum, I. T.; Janik, M. J. The Impact of Specifically Adsorbed Ions on the Copper-Catalyzed Electroreduction of CO2. *J. Electrochem. Soc.* **2016**, *163*, F477−F484.

(24) Murata, A.; Hori, Y. Product Selectivity Affected by Cationic Species in Electrochemical Reduction of CO2 and CO at a Cu Electrode. *Bull. Chem. Soc. Jpn.* **1991**, *64*, 123−127.

(25) Resasco, J.; Chen, L. D.; Clark, E.; Tsai, C.; Hahn, C.; Jaramillo, T. F.; Chan, K.; Bell, A. T. Promoter Effects of Alkali Metal Cations on the Electrochemical Reduction of Carbon Dioxide. *J. Am. Chem. Soc.* **2017**, *139*, 11277−11287.

(26) Varela, A. S.; Ju, W.; Reier, T.; Strasser, P. Tuning the Catalytic Activity and Selectivity of Cu for CO2 Electroreduction in the Presence of Halides. *ACS Catal.* **2016**, *6*, 2136−2144.

(27) Kim, B.; Ma, S.; Molly Jhong, H.-R.; Kenis, P. J. A. Influence of dilute feed and pH on electrochemical reduction of CO 2 to CO on Ag in a continuous flow electrolyzer. *Electrochim. Acta* **2015**, *166*, 271−276.

(28) Gao, D.; Wang, J.; Wu, H.; Jiang, X.; Miao, S.; Wang, G.; Bao, X. pH effect on electrocatalytic reduction of CO2 over Pd and Pt nanoparticles. *Electrochem. Commun.* **2015**, *55*, 1−5.

(29) Ma, M.; Djanashvili, K.; Smith, W. A. Controllable Hydrocarbon Formation from the Electrochemical Reduction of CO2 over Cu Nanowire Arrays. *Angew. Chem.* **2016**, *128*, 6792−6796.

(30) Varela, A. S.; Kroschel, M.; Reier, T.; Strasser, P. Controlling the selectivity of CO2 electroreduction on copper: The effect of the electrolyte concentration and the importance of the local pH. *Catal. Today* **2016**, *260*, 8−13.

(31) Raciti, D.; Mao, M.; Park, J. H.; Wang, C. Local pH Effect in the CO2Reduction Reaction on High-Surface-Area Copper Electrocatalysts. *J. Electrochem. Soc.* **2018**, *165*, F799−F804.

(32) Ryu, J.; Wuttig, A.; Surendranath, Y. Quantification of Interfacial pH Variation at Molecular Length Scales Using a Concurrent Non-Faradaic Reaction. *Angew. Chem., Int. Ed.* **2018**, *57*, 9300−9304.

(33) Rosen, B. A.; Salehi-Khojin, A.; Thorson, M. R.; Zhu, W.; Whipple, D. T.; Kenis, P. J.; Masel, R. I. Ionic liquid-mediated selective conversion of CO(2) to CO at low overpotentials. *Science* **2011**, *334*, 643−644.

(34) Asadi, M.; Kim, K.; Liu, C.; Addepalli, A. V.; Abbasi, P.; Yasaei, P.; Phillips, P.; Behranginia, A.; Cerrato, J. M.; Haasch, R.; Zapol, P.; Kumar, B.; Klie, R. F.; Abiade, J.; Curtiss, L. A.; Salehi-Khojin, A. Nanostructured transition metal dichalcogenide electrocatalysts for CO2 reduction in ionic liquid. *Science* **2016**, *353*, 467−470.

(35) Neubauer, S. S.; Krause, R. K.; Schmid, B.; Guldi, D. M.; Schmid, G. Overpotentials and Faraday Efficiencies in CO2 Electrocatalysis-the Impact of 1-Ethyl-3-Methylimidazolium Trifluoromethanesulfonate. *Adv. Energy Mater.* **2016**, *6*, 1502231.

(36) Asadi, M.; Kumar, B.; Behranginia, A.; Rosen, B. A.; Baskin, A.; Repnin, N.; Pisasale, D.; Phillips, P.; Zhu, W.; Haasch, R.; Klie, R. F.;

Kral, P.; Abiade, J.; Salehi-Khojin, A. Robust carbon dioxide reduction on molybdenum disulphide edges. *Nat. Commun.* **2014**, *5*, 4470.

(37) Zhuang, T.-T.; Liang, Z.-Q.; Seifitokaldani, A.; Li, Y.; De Luna, P.; Burdyny, T.; Che, F.; Meng, F.; Min, Y.; Quintero-Bermudez, R.; Dinh, C. T.; Pang, Y.; Zhong, M.; Zhang, B.; Li, J.; Chen, P.-N.; Zheng, X.-L.; Liang, H.; Ge, W.-N.; Ye, B.-J.; Sinton, D.; Yu, S.-H.; Sargent, E. H. Steering post-C−C coupling selectivity enables high efficiency electroreduction of carbon dioxide to multi-carbon alcohols. *Nat. Catal.* **2018**, *1*, 421−428.

(38) Dinh, C. T.; Burdyny, T.; Kibria, M. G.; Seifitokaldani, A.; Gabardo, C. M.; Garcia de Arquer, F. P.; Kiani, A.; Edwards, J. P.; De Luna, P.; Bushuyev, O. S.; Zou, C.; Quintero-Bermudez, R.; Pang, Y.; Sinton, D.; Sargent, E. H. CO2 electroreduction to ethylene via hydroxide-mediated copper catalysis at an abrupt interface. *Science* **2018**, *360*, 783−787.

(39) Trasatti, S.; Petrii, O. A. Real surface area measurements in electrochemistry. *J. Electroanal. Chem.* **1992**, *327*, 353−376.

(40) Clark, E. L.; Resasco, J.; Landers, A.; Lin, J.; Chung, L.-T.; Walton, A.; Hahn, C.; Jaramillo, T. F.; Bell, A. T. Standards and Protocols for Data Acquisition and Reporting for Studies of the Electrochemical Reduction of Carbon Dioxide. *ACS Catal.* **2018**, *8*, 6560−6570.

(41) Kang, Y.; Yang, P.; Markovic, N. M.; Stamenkovic, V. R. Shaping electrocatalysis through tailored nanomaterials. *Nano Today* **2016**, *11*, 587−600.

(42) Strasser, P.; Gliech, M.; Kuehl, S.; Moeller, T. Electrochemical processes on solid shaped nanoparticles with defined facets. *Chem. Soc. Rev.* **2018**, *47*, 715−735.

(43) Callejas, J. F.; Read, C. G.; Roske, C. W.; Lewis, N. S.; Schaak, R. E. Synthesis, Characterization, and Properties of Metal Phosphide Catalysts for the Hydrogen-Evolution Reaction. *Chem. Mater.* **2016**, *28*, 6017−6044.

(44) Niu, Z.; Becknell, N.; Yu, Y.; Kim, D.; Chen, C.; Kornienko, N.; Somorjai, G. A.; Yang, P. Anisotropic phase segregation and migration of Pt in nanocrystals en route to nanoframe catalysts. *Nat. Mater.* **2016**, *15*, 1188−1194.

(45) Cui, C.; Gan, L.; Heggen, M.; Rudi, S.; Strasser, P. Compositional segregation in shaped Pt alloy nanoparticles and their structural behaviour during electrocatalysis. *Nat. Mater.* **2013**, *12*, 765−771.

(46) Stamenkovic, V. R.; Mun, B. S.; Arenz, M.; Mayrhofer, K. J.; Lucas, C. A.; Wang, G.; Ross, P. N.; Markovic, N. M. Trends in electrocatalysis on extended and nanoscale Pt-bimetallic alloy surfaces. *Nat. Mater.* **2007**, *6*, 241−247.

(47) Zhu, W.; Michalsky, R.; Metin, O.; Lv, H.; Guo, S.; Wright, C. J.; Sun, X.; Peterson, A. A.; Sun, S. Monodisperse Au Nanoparticles for Selective Electrocatalytic Reduction of CO2 to CO. *J. Am. Chem. Soc.* **2013**, *135*, 16833−16836.

(48) Zhu, W.; Zhang, Y. J.; Zhang, H.; Lv, H.; Li, Q.; Michalsky, R.; Peterson, A. A.; Sun, S. Active and selective conversion of CO2 to CO on ultrathin Au nanowires. *J. Am. Chem. Soc.* **2014**, *136*, 16132−16135.

(49) Manthiram, K.; Beberwyck, B. J.; Alivisatos, A. P. Enhanced electrochemical methanation of carbon dioxide with a dispersible nanoscale copper catalyst. *J. Am. Chem. Soc.* **2014**, *136*, 13319−13325.

(50) Loiudice, A.; Lobaccaro, P.; Kamali, E. A.; Thao, T.; Huang, B. H.; Ager, J. W.; Buonsanti, R. Tailoring Copper Nanocrystals towards C2 Products in Electrochemical CO2 Reduction. *Angew. Chem., Int. Ed.* **2016**, *55*, 5789−5792.

(51) Kim, D.; Resasco, J.; Yu, Y.; Asiri, A. M.; Yang, P. D. Synergistic geometric and electronic effects for electrochemical reduction of carbon dioxide using gold-copper bimetallic nanoparticles. *Nat. Commun.* **2014**, *5*, 4948.

(52) Reske, R.; Mistry, H.; Behafarid, F.; Roldan Cuenya, B.; Strasser, P. Particle size effects in the catalytic electroreduction of CO(2) on Cu nanoparticles. *J. Am. Chem. Soc.* **2014**, *136*, 6978−6986.

(53) Li, Y.; Cui, F.; Ross, M. B.; Kim, D.; Sun, Y.; Yang, P. Structure Sensitive CO2 Electroreduction to Hydrocarbons on Ultrathin 5-fold Twinned Copper Nanowires. *Nano Lett.* **2017**, *17*, 1312−1317.

(54) Hori, Y.; Takahashi, I.; Koga, O.; Hoshi, N. Selective Formation of C2 Compounds from Electrochemical Reduction of CO2 at a Series of Copper Single Crystal Electrodes. *J. Phys. Chem. B* **2002**, *106*, 15−17.

(55) Schouten, K. J. P.; Pérez Gallent, E.; Koper, M. T. M. Structure Sensitivity of the Electrochemical Reduction of Carbon Monoxide on Copper Single Crystals. *ACS Catal.* **2013**, *3*, 1292−1295.

(56) Roberts, F. S.; Kuhl, K. P.; Nilsson, A. High Selectivity for Ethylene from Carbon Dioxide Reduction over Copper Nanocube Electrocatalysts. *Angew. Chem.* **2015**, *127*, 5268−5271.

(57) Huang, J.; Hormann, N.; Oveisi, E.; Loiudice, A.; De Gregorio, G. L.; Andreussi, O.; Marzari, N.; Buonsanti, R. Potential-induced nanoclustering of metallic catalysts during electrochemical CO2 reduction. *Nat. Commun.* **2018**, *9*, 3117.

(58) Kim, D.; Xie, C.; Becknell, N.; Yu, Y.; Karamad, M.; Chan, K.; Crumlin, E. J.; Norskov, J. K.; Yang, P. Electrochemical Activation of CO2 through Atomic Ordering Transformations of AuCu Nano-particles. *J. Am. Chem. Soc.* **2017**, *139*, 8329−8336.

(59) Wang, Z.; Yang, G.; Zhang, Z.; Jin, M.; Yin, Y. Selectivity on Etching: Creation of High-Energy Facets on Copper Nanocrystals for CO Electrochemical Reduction. *ACS Nano* **2016**, *10*, 4559−4564.

(60) Spori, C.; Kwan, J. T. H.; Bonakdarpour, A.; Wilkinson, D. P.; Strasser, P. The Stability Challenges of Oxygen Evolving Catalysts: Towards a Common Fundamental Understanding and Mitigation of Catalyst Degradation. *Angew. Chem., Int. Ed.* **2017**, *56*, 5994−6021.

(61) Goodman, E. D.; Schwalbe, J. A.; Cargnello, M. Mechanistic Understanding and the Rational Design of Sinter-Resistant Hetero-geneous Catalysts. *ACS Catal.* **2017**, *7*, 7156−7173.

(62) Manthiram, K.; Surendranath, Y.; Alivisatos, A. P. Dendritic assembly of gold nanoparticles during fuel-forming electrocatalysis. *J. Am. Chem. Soc.* **2014**, *136*, 7237−7240.

(63) Kim, D.; Kley, C. S.; Li, Y.; Yang, P. Copper nanoparticle ensembles for selective electroreduction of CO2 to C2-C3 products. *Proc. Natl. Acad. Sci. U. S. A.* **2017**, *114*, 10560−10565.

(64) Hammer, B.; Norskov, J. K. Why gold is the noblest of all the metals. *Nature* **1995**, *376*, 238−240.

(65) Cargnello, M.; Chen, C.; Diroll, B. T.; Doan-Nguyen, V. V.; Gorte, R. J.; Murray, C. B. Efficient removal of organic ligands from supported nanocrystals by fast thermal annealing enables catalytic studies on well-defined active phases. *J. Am. Chem. Soc.* **2015**, *137*, 6906−6911.

(66) Shaw, S.; Tian, X.; Silva, T. F.; Bobbitt, J. M.; Naab, F.; Rodrigues, C. L.; Smith, E. A.; Cademartiri, L. Selective Removal of Ligands from Colloidal Nanocrystal Assemblies with Non-Oxidizing He Plasmas. *Chem. Mater.* **2018**, *30*, 5961−5967.

(67) Aran-Ais, R. M.; Yu, Y.; Hovden, R.; Solla-Gullon, J.; Herrero, E.; Feliu, J. M.; Abruna, H. D. Identical Location Transmission Electron Microscopy Imaging of Site-Selective Pt Nanocatalysts: Electrochemical Activation and Surface Disordering. *J. Am. Chem. Soc.* **2015**, *137*, 14992−14998.

(68) Cao, Z.; Kim, D.; Hong, D.; Yu, Y.; Xu, J.; Lin, S.; Wen, X.; Nichols, E. M.; Jeong, K.; Reimer, J. A.; Yang, P.; Chang, C. J. A Molecular Surface Functionalization Approach to Tuning Nano-particle Electrocatalysts for Carbon Dioxide Reduction. *J. Am. Chem. Soc.* **2016**, *138*, 8120−8125.

(69) Li, D.; Wang, C.; Tripkovic, D.; Sun, S.; Markovic, N. M.; Stamenkovic, V. R. Surfactant Removal for Colloidal Nanoparticles from Solution Synthesis: The Effect on Catalytic Performance. *ACS Catal.* **2012**, *2*, 1358−1362.

(70) Ross, F. M. Opportunities and challenges in liquid cell electron microscopy. *Science* **2015**, *350*, aaa9886.